

A Novel AFM Imaging Method Based on Liquid Force-Distance Curve Analysis

Xiaozhe Yuan, Yongchun Fang, *Senior Member, IEEE*, and Xiao Ren

Abstract—When atomic force microscopy (AFM) systems are employed for scanning tasks in liquid, unexpected nonlinearity caused by laser refraction leads to the distortion of AFM images. A novel liquid imaging method is proposed for high-speed AFM systems. Specifically, imaging signal compensation based on liquid force curve analysis is obtained to remedy the distortion from refraction nonlinearity; and then considering the dynamic characteristics of piezo scanner, which limits the performance of high-speed imaging, the dynamic model of piezo scanner in Z-axis is utilized to improve the AFM's imaging accuracy during high-speed scanning. Experimental results are provided to illustrate the efficacy of proposed liquid imaging method.

I. INTRODUCTION

NANO science and technology have been one of the most cutting-edge research fields today, some unique properties of material in nano-scale have attracted people's attention [1-3]. However the traditional microscopy instruments could hardly meet the demands of observation and manipulation in nano-scale. In 1982, Binning and Rohrer invented the scanning tunneling microscope (STM) [4]. Atomic force microscope (AFM) has been invented as another nano-scale microscopy on the basis of STM, which overcomes the weakness of STM that it can't examine insulated samples [5]. With people's deep understanding of the micro-world, AFM is expected to meet the increasing demands from such fields as life science and chemistry, which are primarily embodied in faster scanning rate, higher resolution, larger scanning range and higher intelligence. Therefore, more and more attention has been paid on improving the performance of AFM itself.

According to statistics, 40 percent applications of AFM are accomplished in liquid [6]. However, researches on AFM system in liquid is very deficient than which in the air. In some cases, it is necessary to examine the samples in liquid, for instance, some biological samples can't maintain biological activities divorced from liquid circumstance, and some electrochemical reactions can only be observed in liquid. In [7], a high-speed AFM system is utilized to conduct single-molecule imaging on living bacterial cell surface. In [8], the contact mode AFM is applied in aqueous medium for

structural analysis of spinach photosynthetic complexes. To investigate the corrosion process of aluminum thin film in pure water, a liquid AFM was invented in [9], their work is mainly focused on the improvement of mechanical and hardware structure.

High precision imaging is expected when supervising some chemical or biological processes in liquid, especially for fast scanning tasks. However, liquid imaging precision is influenced by a number of factors. Firstly, the liquid surface causes the detecting laser beam to refract when it travels through the liquid-air interface. And the refraction causes the magnification varying dynamically during the scanning process. On the other hand, the vibration of the liquid leads to the decreasing of signal to noise ratio of the control error. On the other hand, it is also expected that the imaging precision remains high with the increasing of scanning speed. Many efforts have been made to improve the imaging performance of the AFM system. In [10], parallel scanning method was proposed by installing the 1*2 array cantilever in AFM scanning head. Multiple lines are under scanning simultaneously to improve the scanning speed drastically. In [11], an AFM surface topography observer based on disturbance observer theory was proposed which limited the control error effectively in high-speed scanning, the high-quality is obtained with the surface topography observer simultaneously. In [12], Ragazzon et al. elaborated their transient imaging theory based on estimation of state and parameters. As the most commonly used actuator of AFM systems, the dynamic characteristics of piezo scanner is the critical factor that limiting the response speed of the instrument, the modeling of piezoelectric positioning stage is accomplished in [13], a dynamic imaging method is proposed based on the analysis for the experimental step-response in [14], which achieves superior imaging performance.

In the majority of commercial liquid AFM systems, the nonlinearity of laser displacement detector due to refraction of the laser beam is neglected, which causes detector's magnification varying dynamically during scanning and makes the traditional imaging method inapplicable. In this paper, the refraction is investigated penetratingly, and a theoretical model is developed to analyse how the detector's nonlinearity impact the liquid imaging system. Furthermore, the liquid force curve analysis is utilized to accomplish the compensation of refraction nonlinearity. The dynamic characteristics of piezo scanner is also considered to improve

This work was supported by National Natural Science Foundation (NNSF) of China under Grant 61325017.

The authors are with the Institute of Robotics and Automatic Information System, Nankai University, Tianjin 300071, China, and the Tianjin Key Laboratory of Intelligent Robotics, Tianjin 300071, China (emails: yuanxz@mail.nankai.edu.cn; fangyc@nankai.edu.cn; renx@mail.nankai.edu.cn).

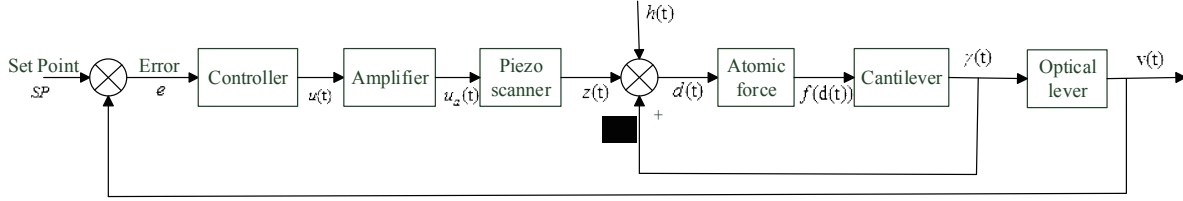


Fig. 1. Control block diagram of AFM in Z-axis.

the image quality in high speed scanning. Some experiments are conducted to illustrate the performance of proposed liquid imaging method.

The remainder of this paper is organized as follows. Section 2 gives a brief introduction to the AFM imaging system and develops the model of refraction nonlinearity. In

section 3, a novel dynamic imaging method in liquid is proposed on the basis of liquid force curve analysis. Section 4 shows some experimental results to illustrate the efficacy of the proposed method. Section 5 is the conclusion of this paper.

II. AFM IMAGING SYSTEM IN LIQUID

A. Conventional Imaging Method

Fig.1 shows the typical control block diagram of AFM in Z-axis, the control system is composed of a piezo-scanner, a micro-cantilever/probe system, a laser displacement detector (optical lever) and a feedback control loop.

Where $u(t)$ denotes the control input of Z-controller, $u_a(t)$ denotes the actual amplified voltage that drives the piezo tube, $z(t)$ denotes the displacement of piezo tube in Z-axis, $d(t)$ denotes the distance between the sample and the probe. The change of atomic force $f(d(t))$ exerts on micro-cantilever leads to a tiny deflection $\gamma(t)$, which is detected by the optical lever and converted into laser spot voltage $v(t)$ by PSD (System output).

When the performance of feedback controller is ideal, control input tracks the sample topography perfectly, the wave-form of control input contains the sample's topography information. The controller's performance gets poorer when increasing scanning rate, control input needs to be compensated to guarantee imaging quality, laser spot voltage (system output) is utilized to improve the performance of whole imaging system. So, conventional imaging method is derived as follow:

$$h = k \cdot (-u + v / k_{sens}). \quad (1)$$

where u denotes the control input, v denotes the system output, k denotes the extension coefficient of piezo-tube in Z-axis and k_{sens} denotes the open loop gain from control signal u to system output v , which is known more commonly as the sensitivity of the AFM system. Dynamic characteristics of piezo scanner is not considered in the conventional imaging method, hence static imaging method is a proper name for it. Fig. 2 shows the schematic diagram of the static imaging method.

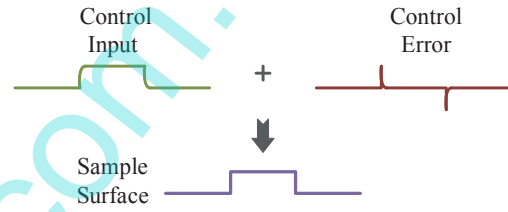


Fig. 2. Schematic diagram of static imaging method.

B. Influencing Factors in Liquid Imaging

There is a subtle difference between operating the AFM system in liquid and in air. However, some factors could be very critical in liquid scanning and we need to give a brief description about these terms which impact the imaging effect in liquid.

Firstly, when the AFM system is operated in the air, hydrophilic sample surfaces will be masked by the water vapor film with prolonged air exposure, the surface tension caused by the film will worsen imaging quality and even snap the probe. Surface tension caused by the water vapor film is eliminated in liquid AFM system since the sample is totally immersed in water.

Secondly, quality factor Q of the scanning probe decreases significantly in liquid, which influences the non-contact mode imaging negatively. Apart from above, detecting laser beam travels through the gas-liquid interface and causes the refraction and reflection, the vibration of liquid surface and refraction of laser beam should also be considered.

Fig.3 shows the light path of detecting laser beam in liquid, vibration of liquid surface caused by air flow and other inevitable external vibration brings obviously random noise in laser spot voltage (system output), reduces the signal to noise ratio significantly.

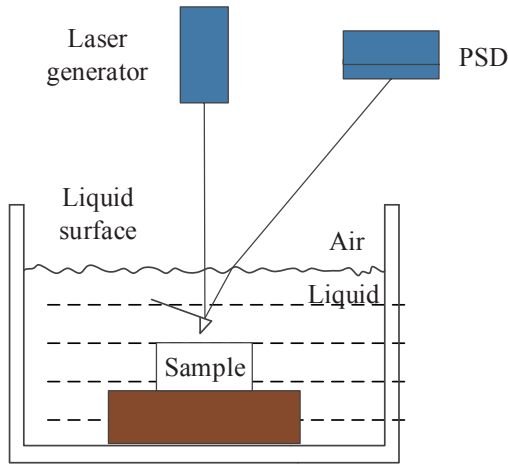


Fig. 3. Light path in liquid.

Liquid surface vibration can be eliminated by refitting the conventional mechanical structure of scanning probe head. By installing a transparent glass window at the liquid-air boundary, light path of laser beam travels through both air-solid and solid-liquid surfaces. Solid window eliminates the random vibration of liquid surface and enhances the signal to noise ratio effectively. Light path with transparent glass window is shown in figure. 4.

C. Modeling of Refraction Nonlinearity

Both reflection and refraction occur when laser beam travels through air-solid and solid-liquid interfaces. Total light intensity reduces as a result of reflection which leads to a large descent of laser spot voltage, the magnification of laser displacement detector decreases synchronously.

Refraction makes the optical lever represents a nonlinear characteristics. In practical situations, detection laser beam travels through both solid-liquid and gas-solid interfaces, to illustrate how refraction of liquid surface makes the magnification of optical lever nonlinear, it is assumed that the laser beam travels through liquid-gas interface only.

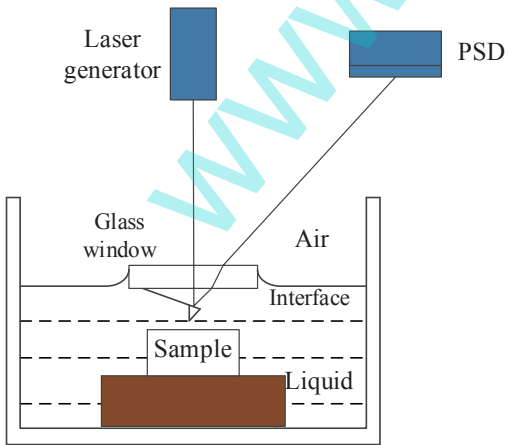


Fig. 4. Light path with transparent glass window.

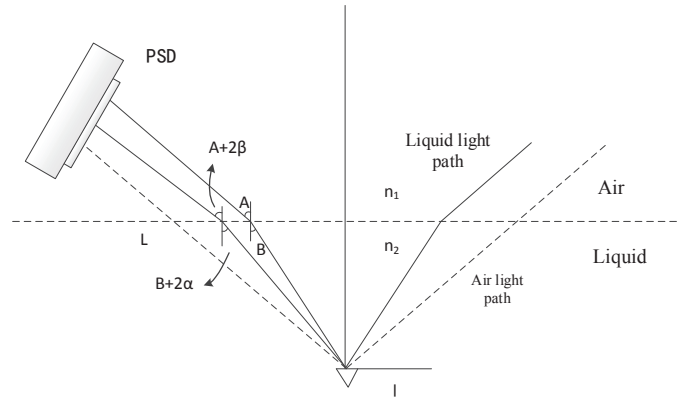


Fig. 5. Schematic diagram of liquid surface refraction

As shown in figure.5, the full line gives the light path of detecting laser beam in liquid, and the dashed line gives the light path in air. n_1 denotes the refractivity in air, n_2 denotes the refractivity in pure water, l denotes the length of micro-cantilever and L denotes the length of reflective laser's light path. A denotes the included angel between laser beam and the normal in the air, B denotes the included angel between laser beam and the normal in liquid.

In air scanning process, micro-cantilever deflects α degree under atomic force. Δz refers to corresponding vertical displacement of probe tip. Deflection angel α of reflection plane (cantilever) leads to a deflection angel 2α of reflective laser. The displacement of laser spot on PSD approximately equals to $2\alpha \cdot L$. The magnification of laser displacement detector in air is derived as follow:

$$\frac{\Delta m}{\Delta z} = \frac{2\alpha L}{\alpha l} = 2L/l. \quad (2)$$

laser beam refracts when travelling through air-liquid interface during liquid scanning, on the basis of refraction's law, it is achieved that:

$$\frac{\sin(A)}{\sin(B)} = \frac{n_2}{n_1}. \quad (3)$$

cantilever deflects α degree, which means the variation of angel B is 2α , corresponding variation of angel A is 2β , using refraction's law again, it is achieved that:

$$\frac{\sin(A+2\beta)}{\sin(B+2\alpha)} = \frac{n_2}{n_1}. \quad (4)$$

the variation of the included angel between the emergent ray and the normal can be derived as follow.

$$2\beta = \arcsin[\sin(B+2\alpha) \cdot \frac{n_2}{n_1}] - A. \quad (5)$$

As shown in fig.5, emergent ray in air scanning and which in liquid scanning are parallel, and light path in liquid is far smaller than which in air. It's a reasonable approximation that light path of reflection laser beam L is fixed. Magnification of optical lever in liquid can be derived as follow, which is obviously nonlinear.

$$\frac{2\beta L}{\alpha l} = \frac{\arcsin[\sin(B+2\alpha) \cdot n_2 / n_1] - A}{\alpha} \cdot \frac{L}{l}. \quad (6)$$

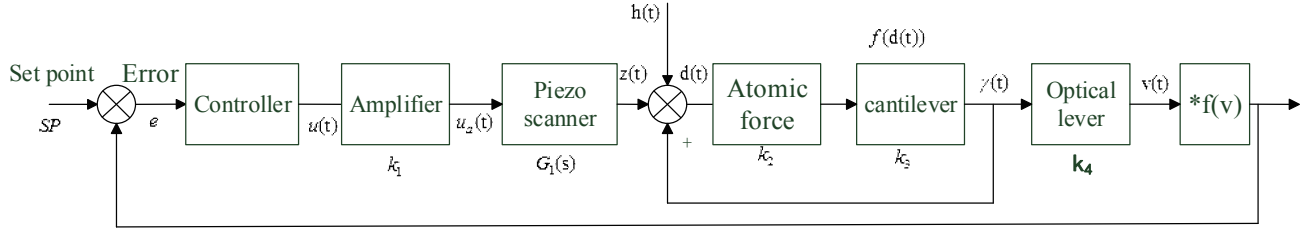


Fig. 6. Liquid phase control block diagram in Z-direction.

where angel B can be replaced by $\arcsin[(n_1/n_2)\sin(A)]$.

Essential parameters in our refraction nonlinearity model consist of the length of cantilever l , the length of reflection laser's light path L , the included angel A between laser beam and the normal in the air and the refractivity in air and liquid. With above analysis, it is demonstrated that liquid surface refraction leads to the nonlinear characteristics of optical lever's magnification. In this scenario, conventional

III. PROCESSING OF LIQUID IMAGING SIGNALS

A. Imaging Compensation Based on Liquid Force Curve

Theoretically, force-distance curve represents the relationship among atomic force and the tip-sample distance. Theoretical force curve is difficult to obtain since the atomic force and the tip-sample distance can't be measured directly.

On the other hand, limited information is contained in theoretical force curve which is only adaptable for qualitative analysis. Meanwhile in practical application, actual force curve refers to the relationship between vertical excitation voltage on piezo scanner and the liquid laser spot voltage. Forward channel of force curve measuring embodies the laser displacement detecting unit (optical lever), hence nonlinear information of optical lever caused by refraction is contained in actual liquid force curve which is worthy of consideration for compensation of the laser spot voltage to improve imaging effect in liquid.

As shown above, conventional imaging method is presented as equation (1), define $k = k_{uz}$, $k/k_{sens} = k_{ez}$, formula above is transformed into:

$$h = -k_{uz} \cdot u + k_{ez} \cdot (v - SP). \quad (7)$$

where k_{uz} denotes the static gain of piezo scanner, k_{ez} denotes the static gain from system output v to the vertical displacement z of the piezo scanner, k_{ez} is regarded as a constant while operating near set point SP in air phase. Furthermore, it is derived that:

$$h = k_{uz} \cdot [-u + (v - SP) / k_{ue}]. \quad (8)$$

where k_{ue} denotes the sensitivity of AFM, namely, the static open-loop gain from control voltage $u(t)$ to laser spot voltage $v(t)$. While scanning in liquid, k_{ue} is variable as a

imaging method may generate significant imaging distortion.

The essence of AFM imaging system is to estimate the sample's topography as precisely as possible with control input $u(t)$ and control output $v(t)$. Both liquid surface refraction and dynamic characteristics of piezo scanner are handled in next section.

result of refraction nonlinearity. Based on the analysis earlier, liquid force curve represents the varying gain from control input system output, assuming that liquid force curve has been derived as $v = f(u)$, corresponding inverse function is $u = f^{-1}(v)$. Substituting the laser spot compensation item $(v - SP) / k_{ue}$ in conventional method with $f^{-1}(v) - f^{-1}(SP)$, static imaging formula in liquid is derived as follow:

$$h = k_{uz} \cdot \{-u + [f^{-1}(v) - f^{-1}(SP)]\}. \quad (9)$$

B. Dynamic Imaging Signal Processing

Majority of commercial AFM products don't take into account the dynamic characteristics of piezo scanner, which is reasonable since residence time of micro probe in each scanning spot suffices for the piezo scanner to reach steady-state. When increasing scanning rate, residence time in each spot is insufficient, hence the dynamic characteristics of piezo tube in Z-axis isn't negligible anymore. Dynamic model of Z-scanner is developed to improve the imaging effect in high-speed scanning.

Fig.6 shows the liquid control block diagram in Z-axis, where k_1 denotes the control input amplifier, k_2 denotes the atomic force coefficient, k_3 denotes the gain of the cantilever and k_4 denotes the gain of the optical lever. Refraction nonlinearity in liquid is equivalent to a varying gain amplifier connected behind the laser displacement detecting unit, $f(v)$ is the amplification coefficient. It is achieved that $f(v) = v / v_L$, where v and v_L denotes laser spot voltages in air and liquid respectively. Similarly, $g(v_L) = v_L / v$.

On the other hand, $G_1(s)$ represents the transfer function of piezo scanner in Z-axis, the output of piezo scanner in Z-axis (i.e. vertical movement) is derived as

$$z(t) = L^{-1}(U(s) \cdot G_1(s)).$$

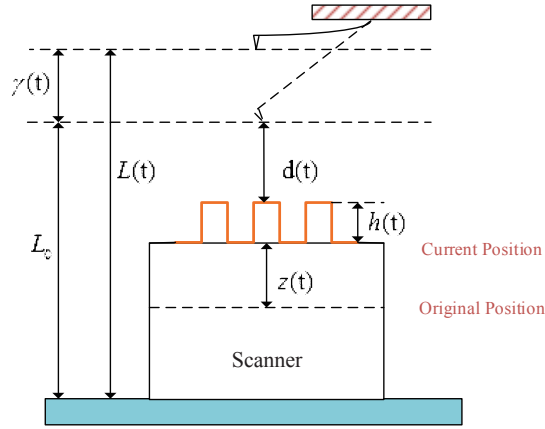


Fig. 7. Positional relationship of probe-sample-scanner system.

Fig.7 is a schematic diagram showing the positional relationship of probe-sample-scanner system, where $\gamma(t)$ denotes the vertical deformation of the probe against original position, $d(t)$ denotes the tip-sample distance and $h(t)$ denotes sample's height. It's obtained that:

$$L_0 + \gamma(t) = d(t) + h(t) + z(t). \quad (10)$$

where $d(0)$ equals to L_0 , then obtain:

$$d(0) + \gamma(t) = d(t) + h(t) + z(t). \quad (11)$$

and the following formula is obtained.

$$\gamma(t) = \Delta d(t) + h(t) + z(t). \quad (12)$$

Dynamic model of piezo scanner in Z-axis is difficult to achieve, the open loop transfer function $G(s)$ of AFM system is utilized to develop the dynamic model of piezo scanner indirectly. Dynamic response of the micro-cantilever/probe module and the optical lever is negligible because their response is much faster than the piezo scanner. From the control block diagram, it's derived that:

$$G(s) = k_1 \cdot k_2 \cdot k_3 \cdot k_4 \cdot G_1(s) \cdot \frac{1}{k_2 k_3 - 1}. \quad (13)$$

The meanings of the parameters are consistent with fig.6, thus, dynamic model of piezo tube in Z-axis is developed as follow:

$$G_1(s) = \frac{k_2 \cdot k_3 - 1}{k_1 \cdot k_2 \cdot k_3 \cdot k_4} G(s). \quad (14)$$

C. Dynamic Imaging Method with Liquid Compensation

According to earlier analysis, topography height is obtained as follow:

$$h(t) = \gamma(t) - z(t) - \Delta d(t). \quad (15)$$

stroke of the piezo-tube in Z-axis is calculated with the dynamic model, hence:

$$\begin{aligned} h(t) &= (k_2 \cdot k_3 - 1) \cdot \Delta d(t) - L^{-1}(U(s) \cdot k_1 \cdot G_1(s)) \\ &= \frac{k_2 k_3 - 1}{k_2 k_3 k_4} \cdot v(t) - \frac{k_2 k_3 - 1}{k_2 k_3 k_4} \cdot L^{-1}(U(s) \cdot G(s)). \end{aligned} \quad (16)$$

considering the varying gain caused by refraction in liquid, $v(t) = v_L(t) \cdot g(v_L(t))$, imaging formula in liquid is achieved :

$$h(t) = \frac{k_2 k_3 - 1}{k_2 k_3 k_4} \cdot g(v_L) \cdot v_L(t) - \frac{k_2 k_3 - 1}{k_2 k_3 k_4} \cdot L^{-1}(U(s) \cdot G(s)). \quad (17)$$

which is simplified as:

$$h(t) = k_v \cdot g(v_L) \cdot v_L(t) - k_v \cdot L^{-1}(U(s) \cdot G(s)). \quad (18)$$

where k_v equals to $(k_2 k_3 - 1) / k_2 k_3 k_4$.

To view the comparison with air imaging formula, the proposed function is converted into following form:

$$\begin{aligned} h(t) &= k_v \cdot g(v_L(t)) - k_v \cdot L^{-1}(U(s) \cdot G(s)) + \\ &\quad k_v \cdot v_L(t) - k_v \cdot v_L(t) \\ &= h'(t) + k_v \cdot v_L(t) \cdot (g(v_L) - 1). \end{aligned} \quad (19)$$

where $h'(t)$ denotes the sample's height calculated with air imaging formula, the second part of the function represents the compensation term of refraction nonlinearity.

To apply the proposed liquid imaging method, the identification of varying gain $g(v_L)$ needs to be accomplished. There is no proper way to obtain $g(v_L)$ directly, further transformation of imaging formula is achieved to utilize the liquid force curve for imaging signal compensation. Fig.8 shows the force curve measured in our laboratory, where the full line gives the force curve in air and the dashed line gives the force curve measured in liquid. Liquid force curve's nonlinear feature is shown clearly which is highly consistent with the previous analysis.

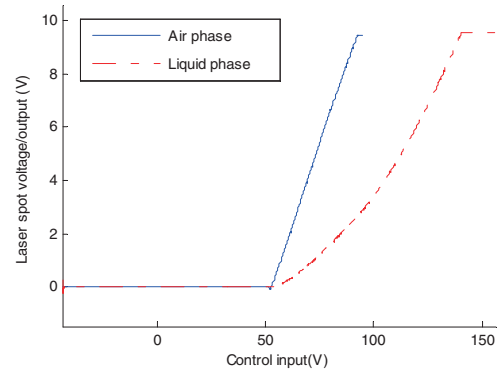


Fig. 8. Liquid/Air force-distance curve.

According to the AFM control diagram, k_v represents the static gain of laser displacement detector and $k_{vz} = k_v = (k_2 k_3 - 1) / k_2 k_3 k_4$. And $k_{uz} = k_1 k_{G_1}$ denotes the static gain from control signal $u(t)$ to piezo tube displacement $z(t)$. The air phase sensitivity k_{sens} represents the static gain from control input $u(t)$ to laser spot voltage (system output) $v(t)$ and $k_{uv} = k_{sens}$, it's also achieved that $k_v = k_{vz} = k_{uz} / k_{uv}$. Then the imaging formula is transformed into:

$$\begin{aligned} h(t) &= -k_v \cdot L^{-1}(U(s)G(s)) + k_v \cdot g(v_L) \cdot v_L(t) \\ &= -\frac{k_{uz}}{k_{uv}} \cdot L^{-1}(U(s)G(s)) + \frac{k_{uz}}{k_{uv}} \cdot g(v_L) \cdot v_L(t). \end{aligned} \quad (20)$$

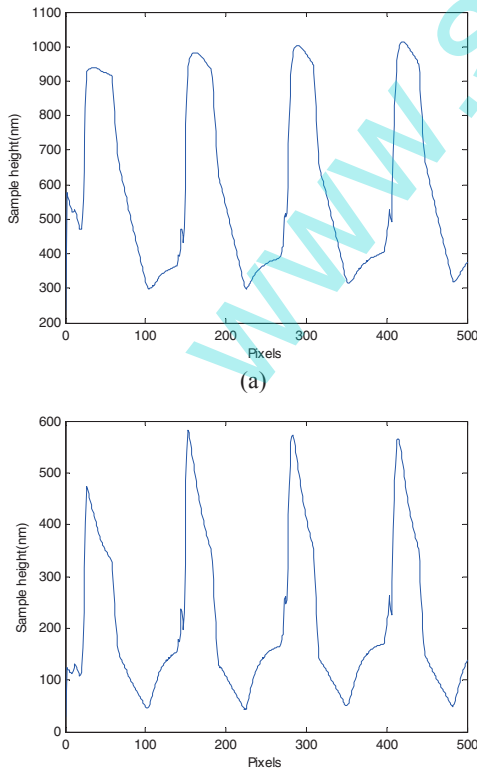
notice that $g(v_L)/k_{uv}$ is the gain from liquid laser spot voltage $v_L(t)$ to control input $u(t)$ and liquid force curve $v_L = \Phi(u)$ is assumed to be achieved, we can derived that:

$$h(t) = -\frac{k_{uz}}{k_{uv}} \cdot L^{-1}(U(s) \cdot G(s)) + k_{uz}[\Phi^{-1}(v_L(t)) - \Phi^{-1}(v_L(0))]. \quad (21)$$

once the liquid force curve is obtained, the formula above can be applied in liquid imaging.

IV. EXPERIMENTAL RESULTS AND ANALYSIS

Some experiments are conducted to illustrate the efficacy of liquid imaging signal compensation. The experimental platform is an AFM system which consists of four parts: a commercial AFM device (CSPM 4000, Being- Nono, Inc., China), a self-designed real-time control module based on RT-Linux. The real-time control system achieves a control period of $50 \mu s$, which is equivalent to a control bandwidth of 20 KHz. As the most typical testing sample, a calibration grating is selected here (TGZ03, μ Masch, Inc., USA). The nominal height of the calibration grating is 500 ± 15 nm. The sample is scanned at the speed of 10 Hz line frequency with the image resolution as 500×500 pixels. The imaging methods here are static methods with and without liquid compensation. As shown in one line topography of calibration grating in fig.9, the conventional method achieves low quality image with severe distortion from original sample, comparatively, one line topography achieved by proposed liquid imaging formula shows the rectangle shape of original sample clearly.



(b)
Fig. 9. One line topography of calibration grating. (a): with liquid signal compensation, (b): without liquid signal compensation.

V. CONCLUSION

Aimed at the problem of operating AFM in liquid, a novel dynamic liquid imaging method is proposed based on liquid force curve analysis. Firstly, analysis on how liquid environment influences the AFM imaging system is carried out theoretically, then the liquid force curve is utilized for the compensation of imaging signals, the dynamic characteristics of piezoelectric actuator are also considered to guarantee the performance of high-speed scanning. A few of experiments are conducted to verify the practical efficacy of proposed liquid imaging method. And the results of the experiments demonstrate that the proposed liquid imaging method obtains sample's topography with less imaging distortion than conventional one.

REFERENCES

- [1] A. L. I. Koochi, H. Hosseini-Toudeshky, and H. R. Ovesy, "Modeling the influence of surface effect on instability of nano-cantilever in presence of van der Waals force," *International Journal of Structural Stability and Dynamics*, vol. 13, no. 4, pp. 756-760, Jul. 2013.
- [2] J. A. Scholl, A. Garcia-Etxarri, and A. L. Koh, "Observation of quantum tunneling between two plasmonic nanoparticles," *Nano letters*, vol. 13, no. 2, pp. 564-569, Mar. 2013.
- [3] J. A. Sichert, Y. Tong, and N. Mutz, "Quantum size effect in organometal halide perovskite nanoplatelets," *Nano letters*, vol. 15, no. 10, pp. 6521-6527, 2015.
- [4] G. Binnig and H. Rohrer, "Scanning tunneling microscopy," *Surface science*, vol. 126, no.1, pp. 236-244, Dec. 1983.
- [5] G. Binnig, C. F. Quate, and C. Gerber, "Atomic force microscope," *Physical review letters*, vol. 56, no. 9, pp. 930-933, Mar. 1986.
- [6] A. M. Baró and R. G. Reifengerger, *Atomic Force Microscopy in Liquid: Biological Applications*, John Wiley & Sons, CA, 2012.
- [7] H. Yamashita, A. Taoka, and T. Uchihashi, "Single-molecule imaging on living bacterial cell surface by high-speed AFM," *Journal of molecular biology*, vol. 422, no. 2, pp. 300-309, 2012.
- [8] W. Phuthong, Z. Huang, and T. M. Wittkopp, "The use of contact mode atomic force microscopy in aqueous medium for structural analysis of spinach photosynthetic complexes," *Plant physiology*, vol. 68, no. 9, pp. 293-299, Mar. 2015.
- [9] H. Zhang, H. Zhang and D. Zhang, "Atomic force microscope measuring in liquid and its applications," *Acta Photonica Sinica*, vol. 33, pp. 1273-1276, 2004.
- [10] X. Lin and W. Dong, "Parallel Scanning of AFM Based on the 1×2 Array Cantilever," *Micronanoelectronic Technology*, vol. 4, no. 7, 2011.
- [11] T. Shiraishi and H. Fujimoto, "High-Speed Atomic Force Microscope by Surface Topography Observer," *Japanese Journal of Applied Physics*, vol. 51, no. 2, pp. 057-063, Mar. 2012.
- [12] M. R. P. Ragazzon, J. T. Gravidahl, K. Y. Pettersen and A. A. Eielson, "Topography and force imaging in atomic force microscopy by state and parameter estimation," in *Proceedings of the 2015 International Conference on American Control Conference*, pp. 3496-3502, June. 2015.
- [13] G. Gu, L. Zhu, C. Su and H. Ding, "Motion Control of Piezoelectric Positioning Stages: Modeling, Controller Design, and Experimental Evaluation," *IEEE/ASME Transactions on Mechatronics*, vol. 18, no. 5, pp. 1459-1471, Oct. 2013.
- [14] X. Ren, Y. Fang, and N. Qi, M. Wu and X. Feng, "A Practical dynamic imaging method for fast-scanning atomic force microscopy," *Instrumentation Science & Technology*, vol.41, no.4, pp. 394-405, 2013.